An Effective Area-based Localization Algorithm for Wireless Networks

Noureddine Lasla, Mohamed F. Younis *Senior Member, IEEE*, Abdelraouf Ouadjaout and Nadjib Badache

Abstract—Area-based localization algorithms use only the position of some reference nodes, called anchors, to estimate the residence area of the remaining nodes. Existing algorithms use a triangle, a ring or a circle as the geometric shape that defines the node's residence area. However, existing algorithms suffer from two major problems: (1) in some cases, they might make wrong decisions about a node presence inside a given area, or (2) they require high anchor density to achieve a low location estimation error and high ratio of localizable nodes. In this paper, we overcome these shortcomings by introducing a new approach for determining the node's residence area that is geometrically shaped as a half-symmetric lens. A novel Half Symmetric Lens based localization algorithm (HSL) is proposed. HSL yields smaller residence areas, and consequently, better location accuracy than contemporary schemes. HSL further employs Voronoi diagram in order to boost the percentage of localizable nodes. The performance of HSL is validated through mathematical analysis, extensive simulations experiments and prototype implementation. The validation results confirm that HSL achieves better location accuracy and higher ratio of localizable nodes compared to competing algorithms.

Index Terms—Localization, Wireless networks, Anchor-based position estimation.

1 Introduction

Localization is one of the technical areas that have received increasing attention in recent years due to the boom in location-based services that mobile users can benefit from and to the wealth of applications of ad-hoc and sensor networks [1], [2], [3]. For example, applications like asset tracking, search and rescue and digital battlefield require the knowledge of node's location in order to achieve the design goal. On the other hand, wireless sensor networks (WSNs) have gained popularity in recent years due to the growing list of applications [4]. Most notable among these applications are those serving in unattended setups where human's presence is risky and/or impractical. Examples include surveillance of vast borders military reconnaissance, and security monitoring of strategic installations. In these applications, battery-operated sensors are randomly deployed in an area to monitor their surroundings and report their findings to a base-station. In order for the sensor data to be considered in situation assessment they need to be correlated to where they are collected from and thus it is important for the location of the individual sensors to be known.

Although GPS receivers would provide a global coordinate system to which the networks node will be related, these receivers require line-of-sight and thus cannot operate in in-door environments and are negatively affected by cloud, terrain and trees [5]. In addition, the small form factor, constrained cost and limited energy supply of the employed nodes make it impractical for each node to have an on-board GPS receiver and the network has to rely on relative localization schemes where a node's position is topologically defined based on proximity to its neighbours and/or reference points. Furthermore, the reliance on WiFi access points and cellular telecommunication structure is impractical or infeasible in many applications of ad-hoc and sensor networks where the network operates using non-standard protocols and within inaccessible deployment area, e.g., in combat field, where telecommunication infrastructure is limited or the use of its service is prohibited.

Localization methodologies can be generally classified into range-free and range-based. Range-based schemes [6], [7], [8] work by measuring point-to-point distance or angle between pairs of communicating nodes, or between a node and an anchor (a reference node with a known position). On the other hand, range-free localization [9], [10], [11], [12], [13] do not require point-to-point measurements and generally uses connectivity to estimate an approximate distance or uses received signal strength indication (RSSI) information to infer the near-far relationships between nodes and anchors, which know their exact position via GPS or manual placement in the field of interest. Most localization schemes provide the coordinates of a node relative to the anchors without bounding the error that these coordinates may be subject to

- *N. Lasla, A. Ouadjabout and N. Badache are with the Center of Research on Scientific & Tech. Info. (CERIST), and the University of Sciences and Technology Houari Boumediene (USTHB), Algeria. E-mail: {n.lasla,a.ouadjaout,badache}@cerist.dz*
- *M. Younis is with Dept. of Computer Science and Elec. Eng., Univ. of Maryland, Baltimore County, Baltimore, MD, USA. E-mail:younis@cs.umbc.edu*

in the x- and y-directions. Area-based localization is a special class of range-free methodologies in which the localization process determines a residence area within which the node is located.

The residence area represents a geographical region containing the node. The process of defining this region for a node involves drawing a set of geometric shapes using the positions of the reachable anchors. Then, the node tests whether it lies inside or outside these geometric shapes. The results of such a test determine the boundary of the node's residence area, i.e., the intersection of shapes that the node is located in and do not overlap with the shapes that do not contain the node. If the node does not belong to any of the formed geometric shapes, it is called non-localizable. Note here that the presence test in area-based approaches relay on the proximity or the near-far information among anchors and nodes. Such information is obtained by using the RSSI measurements from radio transceiver without the need of additional hardware. Some recent studies [11], [12], [14], [15] show that RSSI is an effective metric that indicates near-far relationship, and works well for localization problems especially in outdoor environment. For instance, the experimental results for MICA and MICAz motes reported in [11], [14], show that RSSI values decrease monotonically with increasing distance between the sender and receiver. In addition, a very recent study [16] has demonstrated that it is also possible to indicate near-far relationship among nodes based on RSSI, without extra hardware and even in an environment with obstacles, by using power scanning techniques. The final location of the node can be estimated by computing the centroid of its residence area. The efficiency of the area-based algorithms depends on the size of the calculated residence area; the smaller the size of the area is, the better the accuracy is likely to be.

Area-based localization is deemed effective in applications in which determining the exact position is not a must, the cost and complexity of range estimation hardware is unwarranted, and/or for which the increased communication and computation overhead of multi-literation is not bearable. Examples of these applications include:

1) Secure detention of criminals [17]: A WSN can be used to track inmates inside a large prison by determining the zones within which each inmate is. Area-based location will suffice in detecting any escape attempts and identifying the involved individuals.
2) Livestock Watch [18]: In a cattle grazing field, it is important to track livestock since the grazing field can be close to highways or railroads. Area-based localization can provide an assessment of the safety of the livestock and ensure timely action when one is endangered.

Existing area-based localization algorithms employ one of three types of primitive geometric shapes to draw the nodes' residence areas, namely, a triangle [11], a ring [12], and a circle [13]. However, these algorithms suffer from two major shortcomings. The first is that in some cases, an incorrect decision is made about the presence of a node inside a given area, which affects the correctness of the obtained residence areas. For example, it was shown in [11] that nearly 14% of the decisions made about the presence of a node inside or outside a given triangle are wrong. Meanwhile, to draw the residence area, the authors of [13] assume that the radio propagation model is a perfect circle with known radius. This is an unrealistic assumption [19] and causes major inaccuracy as we illustrate in the next section. The second shortcoming is the need for high anchor density in order to achieve a low localization error and high percentage of localizable nodes. For example, the approaches of [11] and [12] require at least three anchors to draw the node residence area, which means that dense anchor deployment is required to achieve good accuracy and low ratio of non-localizable nodes.

To address the above issues, in this paper we propose a new area-based localization algorithm, called HSL (Half Symmetric Lens based localization algorithm). HSL is based on the geometric shape of half-symmetric lens which can be simply drawn using the location information of only two anchors. Basically, HSL defines the residence area of a node as half of the overlapped area of two circles. As we confirm with detailed mathematical analysis, simulations experiments and prototype implementation, such a residence area is smaller than the one defined by competing-schemes in the literature and thus HSL would yield better location accuracy. To resolve the problem of non-localizable nodes, where a node does hear only from one anchor, HSL uses the Voronoi diagram to divide the network into a set of cells using the communication range of anchors, and locates each node within one Voronoi cell by considering the fact it lies outside the range of anchors that it could not hear from. This allows a non-localizable node to initially define a Voronoi cell as its residence area and then excludes the area covered by unreachable anchors to further diminish the uncertainty about its position.

The rest of the paper is organized as follows. Section 2 discusses the related work. A detailed description of HSL is provided in Section 3. Section 4 derives an analytical estimate of the performance of HSL and compares it to competing schemes. The simulation results are reported in Section 5. Section 6 presents a prototype implementation using MicaZ motes. Finally, Section 7 concludes the paper.

2 Related works

A class of area-based localization schemes relies on received signal strength index (RSSI) measurements

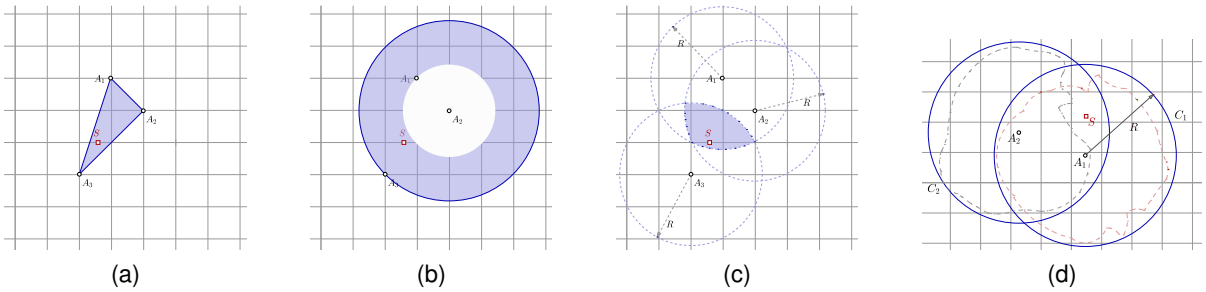

Fig. 1. Basic geometric shape construction in (a) triangle, (b) ring and (c) circle area-based algorithms. (d) Negative information in circular based algorithms

to serve in indoor environments. This class is referred to as fingerprinting and is often applied using WLAN to find the most likelihood area where the node may reside in [20], [21]. A fingerprint is a vector of RSSI measurements using beacons from a set of anchors (access points). First, a map of fingerprints in selected (relatively small) regions in the area of interest is to be prepared through an offline phase where a set of measurements are collected. Interpolation is used to associate a fingerprint to the other regions within the area. To estimate the node residence area, the algorithms tries to find the closest region whose fingerprint closely matches the RSSI values experienced by the node.

Area-based localization schemes determine a residence area where the node lies within, and provide an estimate of the node's position inside such an area. Thus, area-based localization can only give an approximate position with accuracy that depends on the size of the identified residence area; the smaller the size of the area is, the better the localization accuracy would be. The centroid of, or a random point within the residence area may be chosen as a position estimate. The study of [22] shows that the average localization error using the random point may be larger than that of using the centroid based position estimate. Therefore, most of the published area-based algorithms use the centroid method.

The simplest centroid-based scheme has been proposed in [10]. In this algorithm, each anchor transmits a beacon to announce its coordinates. Upon hearing the beacons of neighboring anchors a node calculates the centroid based on the coordinates of these anchors. The main advantage of this solution is its simplicity and ease of implementation. However, this algorithm requires high anchors density in order to ensure that every node hears from multiple anchors. In order to improve the accuracy of the centroid method, more sophisticated algorithms were proposed to shrink the size of the node residence area. The idea is to define a regular geometric shape that defines the coverage of the transmission of anchors. Based on the location of the anchors and their coverage regions, the node checks whether it is located inside or outside these regions. The node's residence area is then defined as the intersection of the coverage regions of the anchors that it hears from. According to the geometric shape of the coverage regions and how they are drawn, we distinguish three classes of algorithms; triangle, ring and circle based.

2.1 Triangle based Algorithms

He et al., [11] have proposed to redraw the node residence area as a set of triangles made up of vertices formed by all the possible subset of three neighbouring anchors (see Fig. 1(a)). By executing the belonging test, which checks whether a node is inside each of the formed triangles or not, the node residence area can be redefined as the intersection of the triangles in which the node resides. A node's presence inside or outside a given triangle, can be assessed using perfect Point In Triangle (PIT) test [11]. If there exists a direction such that a point adjacent to point S is further/closer to points $A1, A2,$ and $A3$ simultaneously, then S is outside the triangle $\triangle A_1A_2A_3$. Otherwise, S is inside $\triangle A_1A_2A_3$. However, in a network with stationary nodes, the perfect PIT test is infeasible since it requires node movement. To deal with this problem, the authors have proposed an Approximate Point In Triangle (APIT) test that uses a neighboring node information to emulate the node movement in perfect PIT test. If no neighbour of S is further from/closer to all three anchors A_1, A_2 and A_3 simultaneously, S assumes that it is inside $\triangle A_1A_2A_3$. Otherwise, S assumes it lies outside this triangle. The proximity assessment information is derived from RSSI exchanged between neighboring nodes. However, by relying only on neighboring nodes the number of emulated direction becomes limited by the number of neighbors and APIT may make an incorrect assessment. It is shown that when the node density per radio range is 6, the percentage of such an assessment error in APIT can reach 14%. Therefore, the accuracy of the estimated position diminishes when the density of nodes is low. Moreover, the APIT test requires exchanging extra RSSI information messages between each node and all its neighbors, i.e., two rounds of broadcast.

2.2 Ring based Algorithms

Liu et al., [12] proposed a localization algorithm called ROCRSSI, which redraws the node residence area

as the overlap of multiple rings. Fig. 1(b) shows an illustration. The belonging test checks the presence of a node S inside a ring formed by the intersection of two concentric circles centred at the point formed by one neighbor anchor A_1. The radius of the inner and the outer circles are the distances between A_1 and two other anchors A_2 and A_3. Based on the comparison of RSSI values between $A_1 - A_2$, $A_1 - A_3$ and $A_1 - S$, the node S can check whether it is inside or outside the formed ring. If $RSSI(A_1, A_2) > RSSI(A_1, S) > RSSI(A_1, A_3)$, then S is likely to fall within the shadowed ring area. This process is repeated for each set of three neighboring anchors, and the final residence area is reduced and formed as the intersection of all the rings that the node falls within. To perform the belonging test, each anchor should inform the nodes of the measured RSSI values with its neighbor anchors. Thus, the extra exchanged RSSI messages and the need of anchors with high power radio transmission, make this scheme unsuitable for resource-constrained networks.

2.3 Circle based Algorithms

In this class of algorithms [13], [23], [24], [25], a node calculates its residence area based on the assumption that the radio coverage area is modelled as a perfect circle with a known radius R. So, each node can deduce whether it is within each of the areas covered by the radio range of its neighbor anchors (see Fig. 1(c)). The overlapping region of all the circles defines the node's residence area. The obtained residence area may also be narrowed-down using the coverage area of farther anchors (anchors within two-hops) which is discarded from the node's residence area since they are not directly reachable.

However, modelling the radio range as a perfect circle with known radius is not realistic and does not often hold in practice. Furthermore, this approach might deem a node non-localizable. For instance, let us consider the example shown in Fig. 1(d). In the figure, the area marked by the dotted lines represents the anchors' practical communication region, while the circle marks the ideal scenario. A node S can hear from anchor A_1, and hence its initial residence area is determined as a circle C_1 centred at A_1 with radius R. The node S discovers a two-hops anchor A_2, and uses this negative information to refine its residence area by discarding the intersection region of the two circles C_1 and C_2, where C_2 is the circle centred at A_2 with radius R. It is clear that S becomes non-localizable as it is outside the refined residence area. Therefore, the negative information can be misleading and might not be helpful in refining the nodes' residence area.

In summary, existing area-based location schemes are prune to increased localization error and requires relatively high count of anchors as most of them require at least three anchors to perform the localization process. The proposed HSL approach opts to overcome these shortcomings as we explain next.

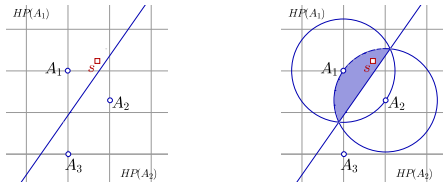

Fig. 2. Overview of the half-symmetric lens construction: (a) node s resides in half plane $HP(A_1)$, (b) node s resides in half-symmetric lens $HSL(A_1, A_2)$

3 HSL-BASED LOCALIZATION

In this section, we present our proposed HSL localization algorithm. HSL avoids the shortcomings of existing schemes by introducing a new shape that leads to a smaller residence area. To localize a node, HSL requires only two neighboring anchors and thus increases the ratio of localizable nodes. To boost this ratio even more, HSL employs a Voronoi diagram based technique. In the balance of this section, nodes are assumed to be randomly deployed and have unique IDs. Each anchor is assumed to know its position and the position of all other anchors.

3.1 Approach Overview

Let $A = \{A_1, A_2, ...A_m\}$ be a set of neighboring anchors of node S in two dimensional Euclidean plane. For any two anchors A_i and A_j, let $B(A_i, A_j)$ be the perpendicular bisector of segment $\overline{A_i\ A_j}$, which divides the plane into two halves HP_{A_i} and HP_{A_j} containing A_i and A_j, respectively. Thus, S is in HP_{A_i} if it is closer to A_i than A_j, or S is in HP_{A_j} if it is closer to A_j than A_i (see Fig. 2(a)). Let us now draw two circles C_{A_i} and C_{A_j} centred at A_i and A_j respectively, with the same radius that equals to the distance d_{ij} between A_i and A_j. The intersection of C_{A_i} and C_{A_j} creates a geometric shape called *symmetric lens* or Vesica piscis [26]. The bisector $B(A_i, A_j)$ divides the symmetric lens into two half-symmetric lens, namely, $HSL(A_i, A_j)$ and $HSL(A_j, A_i)$, containing A_i and A_j, respectively, as depicted in Fig. 2(b). Therefore, (*i*) if S is in $HP(A_i)$, (*ii*) if S is the closer node to A_i than A_j and (*iii*) if S is the closer node to A_j than A_i, then S must be in $HSL(A_i, A_j)$. The same applies for $HP(A_j)$ and A_j. Otherwise, S is outside the symmetric lens $SL(A_i, A_j)$ defined by the coordinate of A_i and A_j. We note that the circles drawn to construct HSL are totally different from those used in the circular-area based algorithms discussed in the previous section.

To derive the near-far information between nodes, we use the Received Signal Strength power as Indicator (RSSI). Formally, a node S is inside the symmetric

lens of two anchors A_i and A_j, if and only if:

$$RSSI_{A_iS} > RSSI_{A_iA_j} \text{ and } RSSI_{A_jS} > RSSI_{A_iA_j}$$

If indeed node S lies in the symmetric lens for the two neighboring anchors A_i and A_j, node S has to find in which sub-area it resides. Basically, if $RSSI_{A_iS} > RSSI_{A_jS}$ node S concludes that is in $HSL(A_i, A_j)$ as illustrated in Fig. 2(b). Otherwise, it is in $HSL(A_j, A_i)$. It is worth noting that the probability of having $RSSI_{A_iS} = RSSI_{A_jS}$ is very minute in practice; nonetheless, if it happens that the node has to be located on the bisector and the accuracy of the estimated coordinates will be quite high. In addition, if the node is not within the symmetric lens area $SL(A_i, A_j)$, then it is in one of the following two geometric area:

1) The node S is inside one of the circles centred at A_i and A_j and not in the symmetric lens $SL(A_i, A_j)$; this area have a *crescent*-like shape and we denote it by CR. Such a scenario can be checked by simply comparing $RSSI_{A_iS}$ and $RSSI_{A_jS}$ to $RSSI_{A_iA_j}$. If the $RSSI_{A_iS} > RSSI_{A_iA_j}$ it could be concluded that S is in the area within the circle of radius d_{ij} centred at A_i minus $SL(A_i, A_j)$, denoted as $CR(A_i, A_j)$. Similarly, if $RSSI_{A_jS} > RSSI_{A_jA_i}$, S would be in $CR(A_j, A_i)$.
2) Otherwise, the node is outside the area defined by the union of the two circles centred at A_i and A_j with the same radius that equals to d_{ij}. We refer to this area as excluded region and we denote it by $ER(A_i, A_j)$.

3.2 Non-localizable Node Problem

Let us consider the example shown in Fig. 3, where A_1 and A_2 are neighbors of node S. We can see that the two circles and the half-symmetric lens area defined by the two anchors A_1 and A_2 do not contain node S. In this situation, node S cannot locates itself even with the presence of two neighboring anchors, and it is considered non-localizable. To overcome this problem, we partition the network area into a set of disjoint regions in such a way to allow node S to locate itself within one of those regions using the information about the anchors which it has heard from. Therefore, a non-localizable node becomes localizable and can use the half-symmetric lens to refine its residence area within the identified regions. The partitioning is based on Voronoi tessellation [27].

Let $A = \{A_1, A_2, ..A_n\}$ be a set of anchors in the two-dimensional bounded network area. The Voronoi cell of an anchor A_i with respect to a set of anchors A, denoted $VN(A_i)$, is the set of points in the plane which are closer to A_i than any anchor in $A \setminus \{A_i\}$. If the Voronoi cell of each anchor is constructed with respect to all other anchors in the network, the set of Voronoi cells will be a partition of the node field.

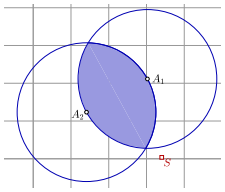

Fig. 3. Illustrating the non-localizable node problem, where the near-far relationship with anchors does not enable node S to determine its residence area with acceptable accuracy

From the above definition, we can conclude that each node is located in the Voronoi cell of its closest anchor (using only one anchor). Using near-far relationship inferred from the RSSI information, each node can determine its closest anchor, and hence the Voronoi cell where it resides in. In this way, each node can locate itself within an initial residence area, i.e., Voronoi cell. After that, the initial residence area will be refined by keeping only the intersection of all the half symmetric lenses that the node belongs to.

3.3 Algorithm Description

At network setup, the individual anchors use the position information to determine the Voronoi cells. The position of anchors can be provided through deterministic placement. Alternatively, an anchor can be equipped with GPS receivers and relatively long haul communication capability so that it can reach other anchors and inform them about its coordinates. The anchor positions are then used to form a Voronoi diagram and determine for each anchor its Voronoi cell. This can be done in a centralized manner or using a distributed algorithm [27], [28], [29].

To perform localization, each anchor starts broadcasting a beacon message containing its coordinates and its Voronoi cell (the coordinates of polygon vertices). Upon receiving the beacon of anchors A, a node S that is within A's reachable range, adds A to its neighbor anchors list denoted by AL_S. Each row in AL_S includes the following information about the neighbor anchor: (1) the anchor's ID, (2) the anchor's coordinates, (3) the anchor's Voronoi cell and (4) the RSSI corresponding to the received beacon message from the anchor.

The Voronoi cell of the nearest anchor, which has the strongest RSSI in AL_S, represents the initial node's residence area. The initial residence area is refined by considering the half symmetric lens, defined based on the coordinates of its neighbor anchors. This process is referred to as the symmetric lens presence test, and involves checking if the node S is inside or outside the symmetric lens area defined by the coordinates of every pair of neighboring anchors. A summary of the HSL presence test is given in Fig. 4.

An example on how the node constructs its residence area is illustrated in Fig. 5. The three anchors A_1, A_2 and A_3 are neighbors of node S, and according to the Voronoi diagram, the network is divided

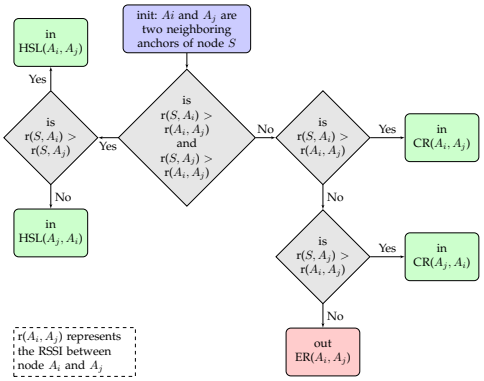

Fig. 4. Flowchart that summarize the HSL presence test

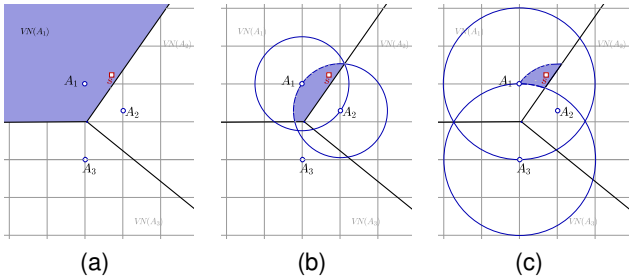

Fig. 5. Residence area construction in HSL: (a) node s is within the $VN(A_1)$, (b) node s in half symmetric lens $HSL(A_1, A_2)$, (c) node s in $HSL(A_1, A_2)$ and not in $SL(A_1, A_3)$

into three sub-areas $VN(A_1)$, $VN(A_2)$ and $VN(A_3)$. Initially, the node S locates itself within the Voronoi cell of its closest anchor $VN(A_1)$ (see Fig. 5(a)). Then, the node S considers $SL(A_1, A_2)$ and $RSSI_{A_1S}$ and $RSSI_{A_2S}$ to conclude that lies inside $HSL(A_1, A_2)$, as shown in Fig. 5(b). The residence area is further refined by considering other anchors. Basically, node S realizes that it is not in the $SL(A_3, A_1)$ (see Fig. 5(c)). This is repeated for all anchors in order to shrink the residence area and increase the localization accuracy. The pseudo code of HSL is provided in Appendix A.

3.4 Estimating Coordinates

In some applications it may be useful to further estimate the coordinates of the node, especially when the residence area of the individual nodes is irregular in shape. Recall that the residence area is defined by the intersection of multiple regular shapes, e.g. a circle, and depends on the location and the size of these regular shapes. Fig. 5 is an example scenario of what a residence area may look like for HSL. To do so, a node S, typically estimates its position as the centroid of the obtained residence area R_S. However, this would involve significantly complex geometry and heavy computation, and may not suit very resource-constrained nodes. To cope with limitation of computation resources, we propose the use of grid scan algorithm to provide an approximate area.

First the initial residence area which is defined by the vertices of the Voronoi cell, is mapped to a grid array. Basically, the smallest rectangle that contains

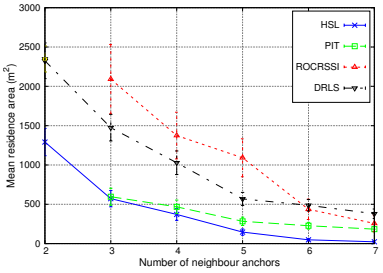

Fig. 6. Average size of the residence area in HSL, PIT, DRLS and ROCRSSI

the Voronoi cell is determined and is divided to small square-shaped cells. The set of grid cells, denoted by G, that the Voronoi cell covers are used to define the residence area. The initial residence area is then refined by excluding cells based on the HSL. Then, the node's position is estimated as the centroid of the grid cells that represent the final residence area. Assume that the grid scanning yields k cells, then the node's coordinates S_e is calculated by:

$$s_e = \{\frac{1}{k}\sum_{i=1}^{k} X_i, \frac{1}{k}\sum_{i=1}^{k} Y_i\}$$

where (X_i, Y_i) are the coordinates of center of cell i of the residence area. Appendix B provides more detailed description of the grid scan algorithm and comparison of its performance to analytical geometry based calculation of the residence area.

4 Performance Analysis

To analyze the performance and assess the advantage of HSL over competing range-free localization scheme, we define the location uncertainty metric as the area that the node's position could be in, i.e., size of the residence area. Obviously, the bigger the residence area is, the higher the level of uncertainty about where the node is located would be, and consequently the lower the localization accuracy would be.

Before analyzing the location uncertainty mathematically, we have first performed an extensive simulation and compared the obtained results with the different area-based approaches discussed in Section 2. In this simulation, the average sizes of the obtained residence area for one node, as a function of the number of its neighboring anchors, are plotted in Fig. 6. The comparison is made with DRLS, ROCRSSI and the perfect version of APIT, namely PIT, which yields better performance than APIT. We have run the simulation 1000 times for each number of neighboring anchors, and the results are plotted with 95% confidence interval. The anchors are deployed inside a circle centred at node's position with radius $R = 40m$ using a uniform random distribution.

From the figure we observe that HSL yields better performance as the average size of the obtained residence area is the smallest under the different number

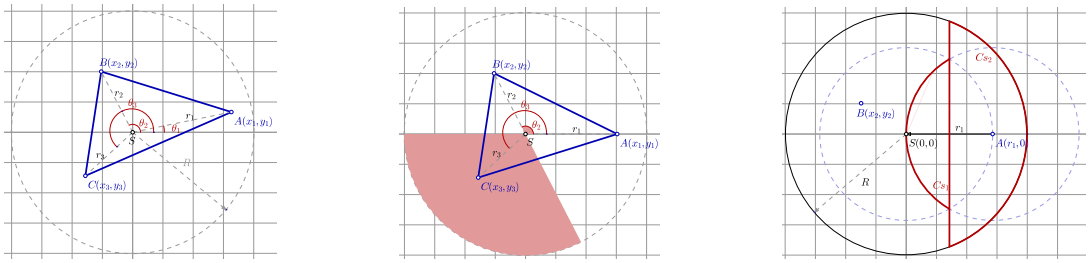

Fig. 7. (a) Polar coordinates representation for the positions of anchors and the node, (b) Condition for a triangle to contains the origin (node), and (c) Condition for an half symmetric lens to contains the origin (node)

of neighboring anchors. The closest performance to HSL is that of PIT, whereas DRLS and ROCRSSI yield weaker performance, and this is due mainly to the basic geometric shape used to draw the residence area in these baseline approaches. To confirm the simulation results in Fig. 6, we conduct mathematical analysis of the size of the residence area in HSL and PIT. We have chosen PIT since it yields better performance than DRLS and ROCRSSI. In the following three subsections, we first derive the expected location uncertainty for PIT in the case where a node has three neighboring anchors. After that, the expected location uncertainty of HSL, when the node has two neighboring anchors, is given. Finally, in the third subsection we make a comparison between the obtained results in order to show which algorithm gives the best performance.

4.1 Expected Location Uncertainty for PIT

In PIT, each node calculates its residence area as the intersection of a set of triangles that contain the node. The size of the intersection area depends on the number of anchors that made the triangles and their position in the plane. In this analysis, we focus on the case of just one triangle when being in the range of three anchors A, B and C, and calculate the expected size of the node residence area as a measure of the location uncertainty metric. Assuming that the position of the three anchors are based on a uniform random distribution within a circle of radius R and centered at the node S, the location uncertainty becomes the expected area of one random triangle inside a circle that contains the origin (i.e., the position of node S), as shown in Fig. 7(a).

The area of a triangle made up of three points $A\ (x_1, y_1)$, $B\ (x_2, y_2)$ and $C\ (x_3, y_3)$ is given by the absolute value of the determinant:

$$T(A,B,C) = \frac{1}{2}\left|\begin{bmatrix} x_1 & y_1 & 1 \\ x_2 & y_2 & 1 \\ x_3 & y_3 & 1 \end{bmatrix}\right| \tag{1}$$

$$T(A,B,C) = \frac{1}{2}(|(x_3y_1) - (x_2y_1) + (x_1y_2) - (x_3y_2) + (x_2y_3) - (x_1y_3)|)$$

Let (r_i, θ_i), $i = 1, 2, 3$ be the polar coordinates of points A, B and C, respectively. Then,

$$x_1 = r_1\cos(\theta_1),\ \ x_2 = r_2\cos(\theta_2),\ \ x_3 = r_3\cos(\theta_3) \tag{2}$$

$$y_1 = r_1\sin(\theta_1),\quad y_2 = r_2\sin(\theta_2),\quad y_3 = r_3\sin(\theta_3) \tag{3}$$

where, $0 \le r_1, r_2, r_3 \le R$ and $0 \le \theta_1, \theta_2, \theta_3 \le 2\pi$.

We look now for the condition that the triangle contains the origin. Because of the symmetry of the system, we can set $\theta_1 = 0$ and $0 \le \theta_2 \le \pi$. For triangle $\triangle(A, B, C)$ to contain the origin, the following two conditions must hold:

- Anchor C must lie on the opposite side of anchor B of the line connecting anchor A and the origin,
- Anchor C must lie on the opposite side of anchor A of the line connecting anchor B and the origin.

In other words, as shown in Fig. 7(b), anchor C must lie in the shaded (red) area, where $\pi \le \theta_3 \le \pi + \theta_2$.

Let P be the probability that a triangle contains the origin. The joint probability distribution function (PDF) of a random point inside a circle (i.e., the joint distributions of random variable X and random variable Y representing the x and y Cartesian coordinate of the random point) is given by:

$$f_{X,Y}(x,y) = \begin{cases} \dfrac{1}{\pi R^2} & \text{if } x^2 + y^2 \le R^2 \\ 0 & \text{otherwise} \end{cases}$$

In a polar coordinate system $r = g_1(x,y) = \sqrt{(x^2+y^2)}$ and $\theta = g_2(x,y) = \arctan(x/y)$. Then, $x = h_1(r,\theta) = r\cos(\theta)$ and $y = h_2(r,\theta) = r\sin(\theta)$. Thus, the joint PDF of a point using the polar coordinate system is given by:

$$f_{R,\Theta}(r,\theta) = f_{X,Y}\left(\ h_1(r,\theta), h_2(r,\theta)\ \right)\ |J(r,\theta)|$$

where $|J(r,\theta)|$ is the Jacobian of the transformation given by:

$$\begin{vmatrix} \partial x/\partial r & \partial x/\partial\theta \\ \partial y/\partial r & \partial y/\partial\theta \end{vmatrix}$$

Then,

$$f_{R,\Theta}(r,\theta) = \begin{cases} \dfrac{r}{\pi R^2} & \text{if } 0 \le \theta \le 2\pi,\ 0 \le r \le R \\ 0 & \text{otherwise} \end{cases}$$

We can rewrite the non-zero part as:

$$f_\Theta(\theta) = \frac{1}{2\pi} \text{ and } f_R(r) = \frac{2r}{R^2}$$

From this, the probability for the triangle to contain the origin is given by:

$$P = \int_0^{\pi} \frac{d\theta_2}{\pi} \int_{\pi}^{\pi+\theta_2} \frac{d\theta_3}{\pi} \iiint_0^R \frac{1}{R^6} 2r_2 2r_2 2r_3 \, dr_1 dr_2 dr_3$$

$$P = \frac{8}{R^6 2\pi\pi} \int_0^{\pi} d\theta_2 \int_{\pi}^{\pi} +\theta_2 d\theta_3 \iiint_0^R r_1 r_2 r_3 dr_1 dr_2 dr_3$$

$$P = \frac{8}{2R^6\pi^2} \frac{\pi^2}{2} (\frac{R^2}{2})^3 = \frac{1}{4}$$

From equations (1), (2) and (3), the area of a triangle using the polar coordinates is given by :

$$T = \frac{1}{2} \left| \begin{bmatrix} r_1\cos(\theta_1) & r_1\sin(\theta_1) & 1 \\ r_2\cos(\theta_2) & r_2\sin(\theta_2) & 1 \\ r_3\cos(\theta_3) & r_3\sin(\theta_3) & 1 \end{bmatrix} \right|$$

The area of a triangle that contains the origin is given by:

$$\begin{aligned} T_0 &= \frac{1}{2} \left| \begin{bmatrix} r_1\cos(0) & r_1\sin(0) & 1 \\ r_2\cos(\theta_2) & r_2\sin(\theta_2) & 1 \\ r_3\cos(\theta_3) & r_3\sin(\theta_3) & 1 \end{bmatrix} \right| \\ &= \frac{1}{2} |r_1 r_2 \sin(\theta_2) - r_2 r_3 \cos(\theta_3)\sin(\theta_2) \\ &\qquad - r_1 r_3 \sin(\theta_3) + r_2 r_3 \cos(\theta_2)\sin(\theta_3)| \\ &= \frac{1}{2} |r_1 r_2 \sin(\theta_2) - r_1 r_3 \sin(\theta_3) + r_2 r_3 \sin(\theta_3 - \theta_2)| \end{aligned}$$

Let G be a random variable that represents the area of a random triangle, and let $\mathscr{C}$ be the event such as the triangle contains the origin. Then the expected value $E(G \mid \mathscr{C})$ is given by:

$$\begin{aligned} &E(G \mid \mathscr{C}) \\ &= \frac{1}{P} \int_{\theta_2=0}^{\pi} \int_{\theta_3=\pi}^{\pi+\theta_2} \iiint_{r_i=0}^R T_0 \; f_R(r_1) \; f_R(r_2) \; f_R(r_3) \\ &f_\Theta(\theta_2) \; f_\Theta(\theta_3) \; dr_1 dr_2 dr_3 \; d\theta_2 d\theta_3 \\ &= \frac{16}{R^6\pi^2} \int_{\theta_2=0}^{\pi} \int_{\theta_3=\pi}^{\pi+\theta_2} \iiint_{r_i=0}^R T_0 \, r_1 r_2 r_3 dr_1 dr_2 dr_3 d\theta_2 d\theta_3 \\ &= \frac{8}{R^6\pi^2} \int_{\theta_2=0}^{\pi} \int_{\theta_3=\pi}^{\pi+\theta_2} \iiint_{r_i=0}^R |r_1 r_2 \sin(\theta_2) - r_1 r_3 \sin(\theta_3) \\ &\qquad + r_2 r_3 \sin(\theta_3 - \theta_2)| \; r_1 r_2 r_3 \; dr_1 dr_2 dr_3 \; d\theta_2 d\theta_3 \end{aligned}$$

Let us calculate the first part of the integral:

$$\begin{aligned} &\int_{\theta_2=0}^{\pi} \int_{\theta_3=\pi}^{\pi+\theta_2} \iiint_0^R r_1 r_2 \sin(\theta_2) \, r_1 r_2 r_3 \, dr_1 dr_2 dr_3 d\theta_2 d\theta_3 \\ &= \int_{\theta_2=0}^{\pi} \int_{\theta_3=\pi}^{\pi+\theta_2} \iiint_{r_i=0}^R r_3 \; r_1^2 r_2^2 \sin(\theta_2) dr_1 dr_2 dr_3 d\theta_2 d\theta_3 \\ &= \int_{\theta_2=0}^{\pi} \int_{\theta_3=\pi}^{\pi+\theta_2} \frac{R^2}{2} \frac{R^3}{3} \frac{R^3}{3} \sin(\theta_2) \quad d\theta_2 d\theta_3 \\ &= \frac{R^8}{18} \int_{\theta_2=0}^{\pi} \int_{\theta_3=\pi}^{\pi+\theta_2} \sin(\theta_2) d\theta_2 d\theta_3 = \frac{R^8}{18} \int_0^{\pi} \theta_2 \sin(\theta_2) d\theta_2 \\ &= \frac{R^8}{18} (-\theta_2\cos(\theta_2) + \; \sin(\theta_2) \;)|_0^{\pi} = \frac{R^8}{18} \; \pi \end{aligned}$$

The other two parts of the integral give the same value. Thus,

$$E(G \mid \mathscr{C}) = |3\frac{R^8}{18} \; \pi \; \frac{8}{R^6\pi^2}| = \frac{4}{3\pi} \; R^2 = 0.424 \; R^2$$

It is worth noting that for $R = 40$ the value matches the one obtained through simulation in Fig. 6 (PIT under 3 anchors).

4.2 Expected Location Uncertainty for HSL

In HSL, the residence area is determined based on the intersection of two circles centered at two anchors A and B with the same radius that is equal to the distance between them d. The intersection should contain the node S. Such intersection represents the location uncertainty of S. As we mentioned earlier, the two anchors lie inside a circle of radius R and centered at S and their positions are determined based on a random uniform distribution. In the following we calculate the expected area of that intersection when it contains the node S, i.e., uncertainty area using just two anchors A and B, and then extend the analysis by factoring in the third anchor C in order to compare with PIT. Again we use $(r_i, \; \theta_i), \; i = 1, \; 2, \; 3$ as the polar coordinates and $(x_i, \; y_i), \; i = 1, \; 2, \; 3$ as the Cartesian coordinates of anchors A, B and C, respectively.

Consider A at distance d from B, the area of the resulting half symmetric lens using A and B, $HSL(A, B)$, is given by: $\frac{1}{2}\left(\frac{2\pi}{3} - \frac{\sqrt{3}}{2}\right) d^2$ [30]. Thus, the expected area of the half symmetric lens that we seek is proportional to the squared distance d^2 between A and B. Let us now derive the condition for $HSL(A, B)$ to contain the origin. Given anchor A at $(r_1, 0)$ (see Fig. 7(c)), it is clear that for $HSL(A, B)$ to contain the origin the following two conditions must be fulfilled:

1) Anchor A must be closer to S than to B, meaning that B must be outside the circle centered at A with radius r_1.
2) Anchor B must be closer to S than to A, which means that B must lie in the side that contains S of the line equidistant from S and A.

Then, the admissible region for B, as shown in Fig. 7(c), is the difference between the whole disc $C(S, R)$ centered at S with radius R and the two red (thick line-marked) circular segments Cs_1 and Cs_2 centered at A and S, respectively.

Thus, the probability P for the intersection to contain S is given by:

$$P = \frac{Area(C(S,R)) - [Area(Cs_1) + Area(Cs_2)]}{Area(C(S,R))}$$

The area of minor segment C_S defined by an angle θ in a circle of radius r is given by:

$$C_S = \frac{1}{2}(\theta - \sin\theta)r^2.$$

For Cs_1, the radius is r_1, $\theta = \frac{2\pi}{3}$ and the area would thus be $\frac{1}{2}(\frac{2\pi}{3} - \frac{\sqrt{3}}{2})r_1^2$. Meanwhile, for Cs_2, the radius is R and $\theta = 2\cos^{-1}\frac{r_1}{2R}$, and thus

$$\begin{aligned} Area(Cs_2) &= \frac{R^2}{2}(\theta - \sin\theta\ ) \\ &= \frac{R^2}{2}\left(2\cos^{-1}\frac{r_1}{2R} - \sin\left(2\cos^{-1}\frac{r_1}{2R}\right)\right) \end{aligned}$$

Substituting

$$\begin{aligned} P = \int_{r_1=0}^{R} \frac{1}{\pi R^2}\Bigg(\pi R^2 - \Bigg(\frac{1}{2}\left(\frac{2\pi}{3} - \frac{\sqrt{3}}{2}\right)r_1^2 \\ + \frac{1}{2}\left(2\cos^{-1}\frac{r_1}{2R} - \sin\left(2\cos^{-1}\frac{r_1}{2R}\right)\right)R^2\Bigg)\Bigg)2r_1\,dr_1 \end{aligned}$$

$$\begin{aligned} P = \frac{2}{\pi R^2}\int_{r_1=0}^{R} \pi R^2 \\ - \left(\frac{1}{2}\left(\frac{2\pi}{3} - \frac{\sqrt{3}}{2}\right)r_1^2 + \frac{1}{2}\left(2\cos^{-1}\frac{r_1}{2R}\right.\right. \\ \left.\left. - \sin\left(2\cos^{-1}\frac{r_1}{2R}\right)\right)R^2\right)r_1 dr_1 \end{aligned}$$

$$P = \frac{3\sqrt{3} + 2\pi}{6\pi} = 0.609$$

The area of the half symmetric lens is given by $\left(\frac{2\pi}{3} - \frac{\sqrt{3}}{2}\right)d^2$ where d is the Euclidean distance between the two anchors A and B. The Euclidean distance d is defined as follow:

$$d^2 = (x_1 - x_2)^2 + (y_1 - y_2)^2$$

Giving anchor A at $(r_1, 0)$

$$d^2 = (r_1 - x_2)^2 + (y_2)^2$$

Let G be a random variable that represents the area of $HSL(A,B)$, and let $\mathscr{C}$ be the event such that the intersection contains the origin. Then, the expected value $E(G \mid \mathscr{C})$ is the integral of the area of HSL over the region satisfying the condition, divided by the probability that $HSL(A,B)$ contains the origin. Let $A_{HSL}(r_1, x_2, y_2)$ denote the area of $HSL(A,B)$. Then

$$\begin{aligned} A_{HSL}(r_1, x_2, y_2) &= \left(\frac{2\pi}{3} - \frac{\sqrt{3}}{2}\right)d^2 \\ &= \left(\frac{2\pi}{3} - \frac{\sqrt{3}}{2}\right)(r_1 - x_2)^2 + (y_2)^2 \end{aligned}$$

Thus,

$$\begin{aligned} &E(G \mid \mathscr{C}) \\ &= \frac{1}{P}\int_{admissible\ region} \mathrm{A_{HSL}}(\mathrm{r_1}, \mathrm{x_2}, \mathrm{y_2})\, f_G(g)\, dg \\ &= \frac{1}{P}\frac{1}{2}\left(\frac{2\pi}{3} - \frac{\sqrt{3}}{2}\right)\int_{admissible\ region} d^2 f_G(g)\, dg \\ &= \frac{1}{P}\frac{1}{2}\left(\frac{2\pi}{3} - \frac{\sqrt{3}}{2}\right)\Bigg(\int_{C(S,R)} d^2 f_G(g)\, dg \\ &\qquad - \left(\int_{CS_1} d^2 f_G(g)\, dg + \int_{CS_2} d^2 f_G(g)\, dg\right)\Bigg) \\ &= \frac{1}{P}\frac{1}{2}\left(\frac{2\pi}{3} - \frac{\sqrt{3}}{2}\right)(I_1 - (I_2 + I_3)) \end{aligned} \tag{4}$$

Where $f_G(g)$ is the probability density function of G given by:

$$\begin{aligned} f_G(g) &= f_R f_X f_Y \\ &= \begin{cases} \frac{2r}{\pi R^2}, & x^2 + y^2 \le R^2 \ and\ 0 \le r \le R \\ 0, & otherwise \end{cases} \end{aligned}$$

From Fig. 7(c) we can derive the bound of the integral as follow:

For $C(S,R)$: $0 \le r_1 \le R$, $-R \le x_2 \le R$ and $-\sqrt{R^2 - x^2} \le y_2 \le \sqrt{R^2 - x^2}$

For $CS_1(A, r_1)$: $0 \le r_1 \le R$, $-r_1 \le x_2 \le -\frac{r_1}{2}$ and $-\sqrt{r_1^2 - x^2} \le y_2 \le \sqrt{r_1^2 - x^2}$

For $CS_2(S,R)$: $0 \le r_1 \le R$, $\frac{r_1}{2} \le x_2 \le R$ and $-\sqrt{R^2 - x^2} \le y_2 \le \sqrt{R^2 - x^2}$

Then,

$$\begin{aligned} I_1 = \frac{1}{\pi R^2}\int_{r_1=0}^{R} 2r_1 dr_1 \int_{x_2=-R}^{R} dx_2 \\ - \int_{y_2=-\sqrt{R^2-x^2}}^{\sqrt{R^2-x^2}} (r_1 - x_2)^2 + (y_2)^2\ dy_2 \\ = R^2 \end{aligned} \tag{5}$$

$$\begin{aligned} I_2 = \frac{1}{\pi R^2}\int_{r_1=0}^{R^2} 2r_1 dr_1 \int_{x_2=-r_1}^{-\frac{r_1}{2}} dx_2 \\ - \int_{y_2=-\sqrt{r_1^2-x^2}}^{\sqrt{r_1^2-x^2}} (0 - x_2)^2 + (y_2)^2\ dy_2 \\ = \frac{1}{144}\left(8 - \frac{3\sqrt{3}}{\pi}\right)R^2 \end{aligned} \tag{6}$$

$$\begin{aligned} I_3 = \frac{1}{\pi R^2}\int_{r_1=0}^{R} 2r_1 dr_1 \int_{x_2=r_{\frac{1}{2}}}^{R} dx_2 \\ - \int_{y_2=-\sqrt{R^2-x^2}}^{\sqrt{R^2-x^2}} (0 - x_2)^2 + (y_2)^2\ dy_2 \\ = \frac{7}{18} - \frac{9\sqrt{3}}{16\pi}R^2 \end{aligned} \tag{7}$$

From equations (4), (5), (6) and (7):

$$E\left(G \mid \delta\right) = \frac{3\left(\frac{1}{144}\left(\frac{3\sqrt{3}}{\pi}-8\right)+\frac{11}{18}+\frac{9\sqrt{3}}{16\pi}\right)\left(\frac{2\pi}{3}-\frac{\sqrt{3}}{2}\right)\pi}{3\sqrt{3}+2\pi}R^2$$

Thus, the expected area of a half symmetric lens that contains the origin is:

$$\frac{(4\pi-3\sqrt{3})(20\pi+21\sqrt{3})}{36(2\pi+3\sqrt{3})}R^2 = \frac{1,769}{2}R^2 = 0.88\ R^2$$

We would like to note that when setting $R = 40$ the value matches the one obtained through simulation in Fig. 6 (HSL under 2 anchors).

4.3 Comparison between HSL and PIT

In the previous two subsections, the expected location uncertainty of PIT and HSL are derived. Because the derivation was under different number of neighboring anchors (three for PIT and two for HSL), the obtained results cannot be directly compared. Therefore, in this subsection, the analysis is extended to compare the expected residence areas based on the same number of anchors.

Let us consider the following assumptions:

1) The deployment region have a rectangular shape $(L \times M)$ of surface D
2) Three anchors A, B and C are deployed in D
3) A node S is deployed in D such as at least two anchors, say A and B, are within its communication range
4) To eliminate the boundary effect, we assume that the node S is deployed in the inner rectangle of the deployment region $(L - R \times M - R)$

We summarize the following probabilities that were derived earlier in this section:

1) $P_n = \pi R^2/D$ is the probability that the anchor C is neighbor of S
2) $P_{HSL(A,B)} = 0.609$ is the probability that node S is within an $HSL(A, B)$
3) $P_{PIT} = 1/4$ is the probability that node S is within triangle $\triangle(ABC)$

To simplify the presentation we set $R = 1$.

4.3.1 The Expected Residence Area in PIT

In PIT, we distinguish between three possible scenarios for residence area for S, according to whether the third anchor C is a neighbor of S and to whether S is within the triangle formed by its three neighboring anchors.

1) The anchor C is not a neighbor of S (Fig. 8(a)). In this case, PIT cannot decides about the position of S, and its residence area will thus be the whole deployment area D.
2) The anchor C is a neighbor of S and S lies within the triangle formed by its three neighbor anchors (Fig. 8(b)). In this case the residence area of S is the triangle $\triangle(A, B, C)$ and its expected area is 0.42 as shown above.
3) The anchor C is a neighbor of S; however S does not lie within the triangle formed by its three neighbor anchors (Fig. 8(c)). In this case, PIT fails to determine the position of S, and its residence area will be the whole deployment area D.

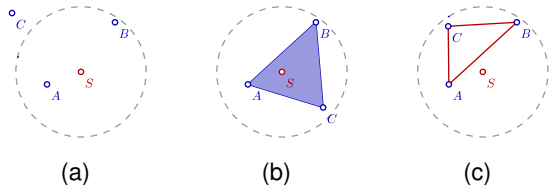

Fig. 8. Possible residences areas in PIT, (a) case 1, (b) case 2 and (c) case 3

The expected node residence area of each of the three enumerated cases in PIT, is the area for each case multiplied by its associated probability of having it.

- Case 1: $D\ (1 - P_n)$
- Case 2: $0.42\ P_n$
- Case 3: $D\ P_n\ (1 - P_{PIT})$

Thus, the expected residence area of PIT in the previous defined network assumptions is given by:

$$E(R_{PIT}) = D\ (1 - P_n) + 0.42\ P_n + D\ P_n\ (1 - P_{PIT})$$

4.3.2 Expected Residence Area in HSL

In HSL we distinguish between four possible cases for the residence areas of S according to whether the third anchor C is located within the range of S, i.e., C is less than R units away from S, and whether S falls within the different formed HSLs using anchors A and B.

1) The anchor C is not a neighbor of S and S is within $HSL(B, A)$ (Fig. 9(a)). For this case the residence area of S is $HSL(B, A)$ and its expected size is 0.88, as shown above in this section.
2) The anchor C is not within the range of S and S does not lie within $HSL(B, A)$ (Fig. 9(b)). In this case the HSL cannot help in determining the position of S, and the residence area would be the whole deployment area D.
3) The anchor C is a neighbor of S and S is within at least one of the three formed HSLs, namely, $HSL(B, A)$, $HSL(B, C)$ or $HSL(A, C)$. This case is illustrated in Fig. 9(c) and for which the size of the residence area is smaller than or equal to 0.88.
4) The anchor C is a neighbor of S and S is not within any of the three formed HSLs, i.e., $HSL(B, A)$, $HSL(B, C)$ and $HSL(A, C)$, as shown in Fig. 9(d). In this case HSL cannot determine the position of S, and its residence area is the whole deployment area D.

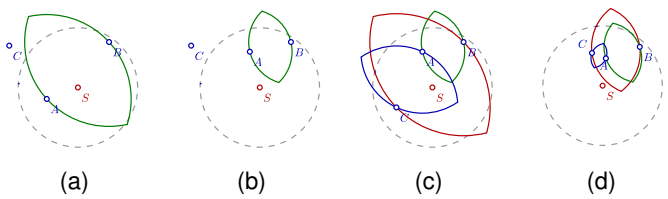

Fig. 9. Possible residences areas in HSL, (a) case 1, (b) case 2, (c) case 3 and (d) case 4

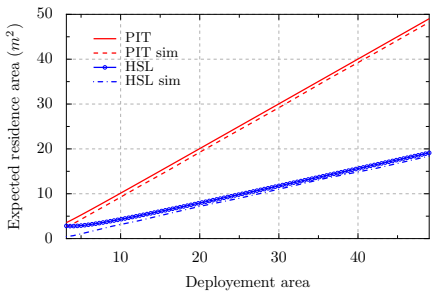

Fig. 10. Validating the analytical performance of HSL and PIT to that obtained through simulation

The expected node residence area of each of the four enumerated cases in HSL, is the area for each case multiplied by the probability of having it.

- Case 1: $0.88\ (1-P_n)$
- Case 2: $D\ (1-P_n)\ (1-P_{HSL(B,A)})$
- Case 3: $0.88\ P_n + 0.88\ P_n + 0.88\ P_n$
- Case 4: $D\ P_n\ (1-P_{HSL(B,A)})\ (1-P_{HSL(B,C)})\ (1-P_{HSL(C,A)})$

Then the upper bound of the expected node residence area for HSL based on the stated network assumptions, is given by:

$$\begin{aligned} E(R_{HSL}) \leq\ & 0.88\ (1-P_n) + D\ (1-P_n)\ (1-P_{HSL(B,A)}) \\ & + 0.88\ P_n + 0.88\ P_n + 0.88\ P_n \\ & + D\ P_n(1-P_{HSL(B,A)})\ (1-P_{HSL(B,C)})\ (1 \\ & - P_{HSL(C,A)}) \end{aligned}$$

In Fig. 10, we plot the expected residence area of both PIT and HSL as a function of D. We plot also the simulation results of both PIT and HSL based on the previously stated network assumptions. We have run the simulation 10000 times for each value of D. In each run the position of the node S and the three anchors are randomly selected and the residence area is calculated based on HSL and PIT. The average over the 10000 runs is plotted in Fig. 10. The simulation results confirm the accuracy of our analysis as the gap between the simulation and analytical results is very small. Fig. 10 also demonstrates the advantage of HSL over PIT where HSL yields localization accuracy that is up to 280% better than PIT.

5 Simulation Experiments

In this section, the performance of HSL is compared through simulation to that of APIT, ROCRSSI and a representative circular-area based algorithm called DRLS [13]. The algorithms are evaluated in terms of the following metrics:

1) **Ratio of localizable nodes**: is defined as the percentage of nodes successfully located within the residence area by the localization algorithm.
2) **Estimation error**: is defined as the average Euclidean distance between the real position of a node and its estimated position.

The performance of HSL is evaluated based on two radio propagation models. The first is the free space model that considers a perfect reception of signals over distance. The second model is the log-distance path loss with shadowing [31], which captures the path loss of RF signals inside a building or in densely populated areas, and formally expressed as:

$$P_{\text{received}}[dBm] = P_{d_0}[dBm] + 10\beta \log_{10}(d/d_0) + X_g \quad (8)$$

where P_{received} is the received power in dBm at distance d, P_{d_0} is the received power at reference distance d_0, β is a path loss exponent and X_g is a Gaussian random variable with zero mean and σ standard deviation. According to [31], a particular environment can be modelled by appropriate setting of β and σ. For this simulation we have considered two settings, urban area $[\beta = 3, \sigma = 5]$ and obstructed factory $[\beta = 4, \sigma = 6.8]$.

In the simulation environment, which is developed in Python , n nodes and m anchors are deployed using a uniform random distribution within an area of size D. We have considered two node densities by changing D, high $(250m \times 250m)$, and low $(400m \times 400m)$. We also study the effect of the ratio of anchors defined as $\frac{m}{m+n}$ in order to assess the resource requirements for the compared approaches. In the simulation results, each plotted point represents the average of 100 executions. We plot the 95% confidence interval on the graphs. The number of nodes and the node's transmission range are set to 300 and $40m$ respectively. We define $\gamma = \frac{R_\alpha}{R_\beta}$ as a parameter in DRLS, where R_α is the communication range set in DRLS, and R_β is the real communication range. As the performance of DRLS depends on γ, which captures the possible incorrect estimation of the actual communication range (R_α), we simulate three versions of DRLS, with $\gamma = 1$, $\gamma = 1.1$ and $\gamma = 1.2$ (hereafter called DRLS-1, DRLS-1.1 and DRLS-1.2, respectively).

5.1 Ratio of Localizable Nodes

Fig. 11 shows the ratio of localizable nodes as a function of the percentage of anchors in the network while assuming a free space model. Figs. 11(a) and 11(b) show that HSL and DRLS-1 yield superior performance that grows as the ratio of anchors increases. This is intuitive as only one anchor is required in HSL and DRLS for a node to determine in which Voronoi cell and circle, respectively, it belongs to. For

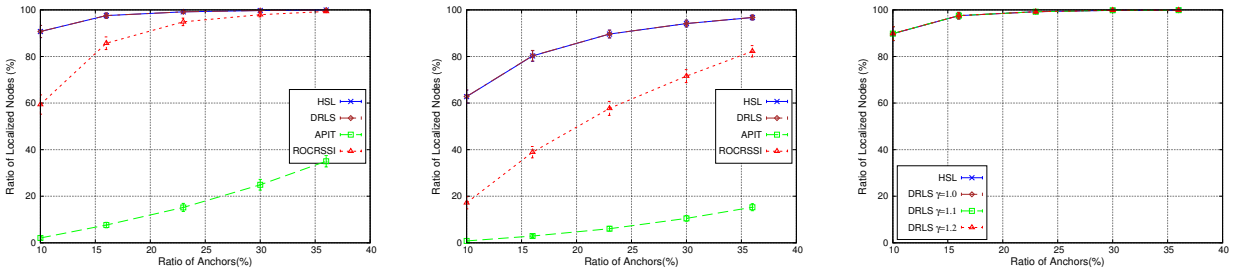

Fig. 11. Localizable nodes ratio assuming a free space model for network size (a) (250×250), (b) (400×400), and (c) DRLS (250×250)

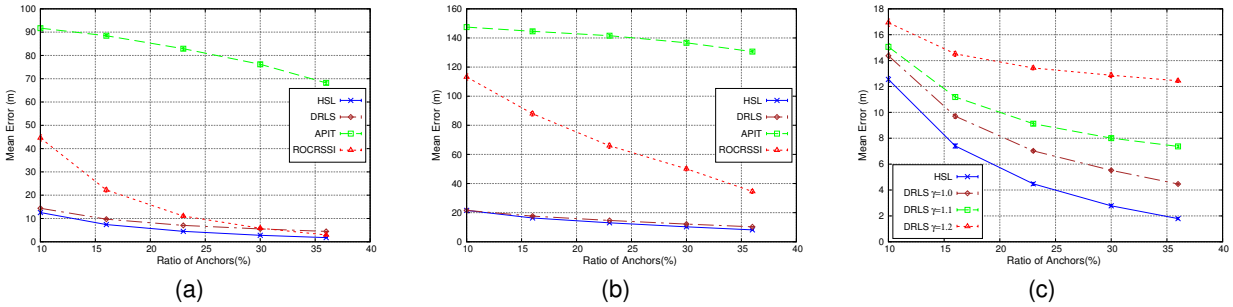

Fig. 12. Average estimation error assuming a free space model for network size (a) (250×250), (b) (400×400), and (c) DRLS (250×250)

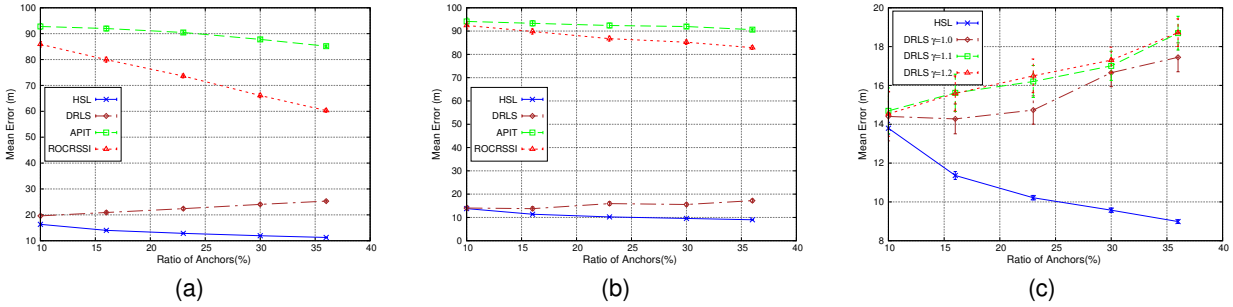

Fig. 13. Average estimation error for log-distance path loss model in (a) urban area, (b) obstructed factory and (c) DRLS in obstructed factory

small ratio of anchors, some nodes may not have any neighboring anchor, and thus become non-localizable. This explains why the ratio of localizable nodes is less than 100% for low anchor count. On the other hand, ROCRSSI and APIT require at least two and three anchors, respectively. In addition, the three anchors in APIT have to form a triangle within which the sensor lies. The same applies to ROCRSSI, whereas the nodes must be within the ring formed by the two anchors. These strong constraints lead to low ratio of localizable nodes. Fig. 11(c) studies the effect of increasing γ on the ratio of localizable nodes in DRLS. As seen in the figure, this ratio is not affected by γ. This is due to the fact that by increasing γ, only the radius of the circle used to estimate the residence area grows. Since the number of neighboring anchors in this case will not be affected, and in DRLS a node needs to hear from at least one anchor to be localizable, the ratio of localizable nodes stays the same. The results about the ratio of localizable nodes in the case of log-distance path loss model are given in Appendix C, where the performances are degraded and more than 20% of nodes become non-localizable.

5.2 Estimation Error

Fig. 12 shows the estimation error as the ratio of anchors varies while assuming a free space model. From Figs. 12(a) and 12(b), we observe that as the ratio of anchors increases, the ratio of localizable nodes increases, and hence lower estimation error is achieved. Also, because the higher number of localizable nodes in HSL and the used geometric shape to determine the residence area, HSL outperforms all the other approaches. In Fig. 12(c), we observe that the estimation error in DRLS grows when γ increases. Higher values of γ imply larger residence area, and hence higher estimation errors are obtained. From the previous two figures, we can note that HSL performs better than DRLS-1, even if they have the same ratio of localizable nodes. This is due to the basic geometric shape used by HSL that yields a smaller residence area. Moreover,

in real deployment setup, it is not possible to perfectly estimate the actual communication range and thus setting γ to 1 is not practical. In Figs. 11(c) and 12(c), the superiority of HSL over DRLS is clearly shown.

Fig. 13 shows the average estimation error in urban area and obstructed factory based on the log-distance path loss model. The results clearly show the negative effect of noises caused by multipath and shadowing on the performance of area based algorithms. Yet the results confirm the advantage of HSL over the other algorithms even in the presence of noises. Fig. 13(c) shows how noises dramatically affect DRLS in the case of incorrect estimation of radio communication range, and confirm the superiority of HSL. Additional simulation results are given in Appendix C.

6 Prototype-based Validation

The efficiency of HSL is further studied through prototype implementation using MEMSIC MicaZ motes [32] equipped with CC2420 RF transceiver [33] and a half-wave external monopole antenna. The transmit power of CC2420 is set to the maximum value 0dBm. The experiment was conducted in an outdoor setup to experience a relatively obstruction-free RF signal propagation. The deployment area was divided into (4×8) grid of squares each of side $2.5m$. In order to avoid ground reflections that produce energy holes, the study in [34] recommends that the heights of the transceiver is to be decreased. To do so while getting accurate RSSI measurements that increase with the distance, placing the transceivers at a height of $0.08m$ was shown to be a good choice. Therefore, we tried heights around such a value and observed the variation of RSSI. Based on multiple trials, the MicaZ motes was finally placed at $0.10m$ from the ground. In the experiment we have deployed 6 MicaZ motes as anchors denoted by A_1, A_2, A_3, A_4, A_5 and A_6 placed at $(2.5, 0)$, $(0, 5)$, $(7.5, 7.5)$, $(2.5, 15)$, $(10, 17.5)$ and $(0, 20)$, respectively. We have also deployed one MicaZ mote as a node denoted by S placed at $(5, 10)$. Node S is to determine its position using the anchors. The anchors start by beaconing their positions. Node S and each anchors record the measured RSSI of all received beacons.

The recorded RSSIs values have then been used to calculate the residence area using both HSL and ROCRSSI. ROCRSSI is picked as a baseline approach in these experiments since its operation requirements is close to those of HSL. Other schemes like PIT requires node movement or a high anchor density to perform the belonging test. To compare the performance of HSL and ROCRSSI under different number of anchors, we execute them for all the possible subset of anchors. In other words, we use all combinations of $2, 3, 4, 5$ and 6 anchors and compare the average size of the residence area for both schemes. The obtained results for each number of anchors are plotted in Fig.

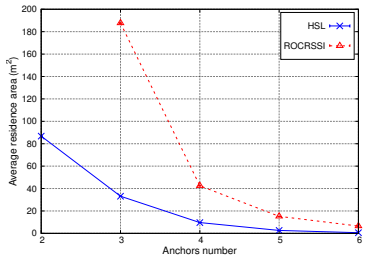

Fig. 14. Average size of the residence area for HSL and ROCRSSI based on experimental results

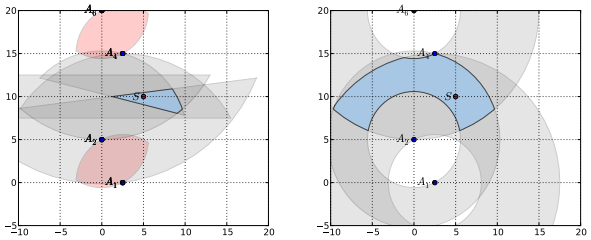

Fig. 15. The obtained residence area in both (a) HSL and (b) ROCRSSI, when the number of anchors is 4

14. From the figure, we can observe that for HSL, the average size of the residence area in the case of two neighboring anchors is about $87m^2$, which is very close to the theoretical analysis result $(0.88\ R^2)$, where $R = 10m$ and presents here the distance between the node S and the farthest anchors A_6. In addition, HSL outperforms ROCRSSI regardless the number of anchors, and yields better results even with few anchors.

An examples of the shapes of the obtained residence area for both HSL and ROCRSSI is shown in Fig. 15. In the figure, the gray areas represents the initial regions where the node is located in, the red areas represents the excluded regions and the blue area represents the final obtained residence area. The size of the residence area in HSL is very small compared to that obtained using ROCRSSI, which confirm the simulation results.

7 Conclusion

In this paper, we have proposed HSL, a new distributed area-based localization algorithm for wireless network. HSL is designed to achieve high ratio of localizable nodes and low error position estimate under lower anchor density compared to the leading schemes in the literature such as APIT, ROCRSSI, and DRLS. HSL is based on the geometric shape of half-symmetric lens which can be simply drawn using only the location information of two anchors. The presence test is based on checking whether a node is within the symmetric lens of different combinations of two neighboring anchors. To resolve the problem of non-localizable nodes, HSL uses the Voronoi diagram to divide the network into a set of cells, and locates each node within one Voronoi cell. This allows a non-

localizable node to use the negative information to diminish its location uncertainty.

The mathematical analysis of the size of the residence area has verified the superior performance of HSL compared to a competing scheme PIT, where HSL yields localization accuracy that is up to 280% better than PIT. Simulation results have also shown that HSL outperforms APIT, ROCRSSI, and DRLS in terms of location accuracy and ratio of localizable nodes. Finally, a prototype implementation using MicaZ motes was performed and the results have confirmed the previous mathematical analysis and simulation experiment.

ACKNOWLEDGMENTS

We would like to thank Prof. Hacene Belbachir for his valuable comments about the theoretical analysis.

REFERENCES

[1] I. Amundson and X. D. Koutsoukos, "A survey on localization for mobile wireless sensor networks," in *MELT*, 2009.
[2] G. Han, H. Xu, J. Jiang, L. Shu, T. Hara, and S. Nishio, "Path planning using a mobile anchor node based on trilateration in wireless sensor networks," *Wireless Communications and Mobile Computing*, vol. 13, no. 14, pp. 1324–1336, 2013.
[3] A. M. Youssef and M. Youssef, "A taxonomy of localization schemes for wireless sensor networks," in *ICWN*, 2007.
[4] T. Arampatzis, J. Lygeros, S. Member, and S. Manesis, "A survey of applications of wireless sensors and wireless sensor networks," in *MED*, 2005, pp. 719–724.
[5] D. K. Petraki, M. P. Anastasopoulos, T. Taleb, and A. V. Vasilakos, "Positioning in multibeam geostationary satellite networks," in *ICC*, 2009, pp. 1–5.
[6] D. Niculescu and B. R. Badrinath, "Ad hoc positioning system (aps) using aoa," in *INFOCOM*, mar 2003.
[7] G. J. Pottie and W. J. Kaiser, "Wireless integrated network sensors," *Commun. ACM*, vol. 43, no. 5, pp. 51–58, 2000.
[8] N. B. Priyantha, A. Chakraborty, and H. Balakrishnan, "The cricket location-support system," in *MOBICOM*, 2000.
[9] D. Niculescu and B. Nath, "Ad hoc positioning system (aps)," in *IN GLOBECOM*, 2001, pp. 2926–2931.
[10] N. Bulusu, J. Heidemann, and D. Estrin, "Gps-less low cost outdoor localization for very small devices," *IEEE Personal Communications Magazine*, vol. 7, no. 5, 2000.
[11] T. He, C. Huang, B. M. Blum, J. A. Stankovic, and T. F. Abdelzaher, "Range-free localization schemes for large scale sensor networks," in *MOBICOM*, 2003, pp. 81–95.
[12] C. Liu, T. Scott, K. Wu, and D. Hoffman, "Range-free sensor localisation with ring overlapping based on comparison of received signal strength indicator," *International Journal of Sensor Networks*, vol. 2, no. 5/6, pp. 399–413, 2007.
[13] J.-P. Sheu, P.-C. Chen, and C.-S. Hsu, "A distributed localization scheme for wireless sensor networks with improved grid-scan and vector-based refinement," *IEEE Transactions on Mobile Computing*, vol. 7, no. 9, pp. 1110–1123, sep 2008.
[14] Z. Z. andTian He, "Rsd: A metric for achieving range-free localization beyond connectivity," *IEEE Trans. Parallel Distrib. Syst.*, vol. 22, no. 11, pp. 1943–1951, 2011.
[15] X. Zhu and G. Chen, "Spatial ordering derivation for one-dimensional wireless sensor networks," in *ISPA*, 2011.
[16] S. T. X. L. X. M. Q. H. C. Bo, D. Ren *et al.*, "Locating sensors in the forest: A case study in greenorbs," in *INFOCOM*, 2012.
[17] W. Zhou, Z. Xuehua, X. Xin, and J. Wu, "The application research of wireless sensor network in the prison monitoring system," in *IITSI*, 2010, pp. 58–62.
[18] J. I. Huircán, C. Muñoz, H. Young, L. Von Dossow, J. Bustos, G. Vivallo, and M. Toneatti, "Zigbee-based wireless sensor network localization for cattle monitoring in grazing fields," *Comput. Electron. Agric.*, pp. 258–264, Nov. 2010.
[19] D. Ganesan, B. Krishnamachari, A. Woo, D. Culler, D. Estrin, and S. Wicker, "Complex behavior at scale: An experimental study of low-power wireless sensor networks," 2002.
[20] E. Elnahrawy, X. Li, and R. P. Martin, "Using area-based presentations and metrics for localization systems in wireless lans," in *LCN*, 2004, pp. 650–657.
[21] Z. Shengliang, W. Bang, M. Yijun, and L. Wenyu, "Indoor multi-resolution subarea localization based on received signal strength fingerprint," in *WCSP*, 2012, pp. 1–6.
[22] S.-G. Zhang, J. Cao, L. C. 0006, and D. Chen, "On accuracy of region-based localization algorithms for wireless sensor networks." in *MASS*, 2009, pp. 30–39.
[23] J.-P. Sheu, J.-M. Li, and C.-S. Hsu, "A distributed location estimating algorithm for wireless sensor networks," in *SUTC (1)*, 2006, pp. 218–225.
[24] Z. Yan, Y. Chang, Z. Shen, and Y. Zhang, "A grid-scan localization algorithm for wireless sensor network," in *CMC (2)*, 2009, pp. 142–146.
[25] T. Kim, M. Son, W. Choi, M. Song, and H. Choo, "Low-cost two-hop anchor node-based distributed range-free localization in wireless sensor networks," in *ICCSA (3)*, 2010, pp. 129–141.
[26] L. Surhone, M. Timpledon, and S. Marseken, *Vesica Piscis: Shape, Circle, Pythagoreanism, Square Root of 3, Continued Fraction, 153, Gospel of John, Miraculous Draught of Fish, Coventry Patmore, New Age, Yoni, Christian Art, Aureola*, 2010.
[27] W. Alsalih, K. Islam, Y. Núñez Rodríguez, and H. Xiao, "Distributed voronoi diagram computation in wireless sensor networks," in *SPAA*, 2008, pp. 364–364.
[28] B. A. Bash and P. J. Desnoyers, "Exact distributed voronoi cell computation in sensor networks," in *IPSN*, 2007, pp. 236–243.
[29] Y. N. Rodríguez, H. Xiao, K. Islam, and W. Alsalih, "A distributed algorithm for computing voronoi diagram in the unit disk graph model," in *CCCG*, 2008.
[30] Area of a symmetric lens (vesica-piscis). [Online]. Available: http://math.ucsd.edu/ wgarner/math4c/randprob/areaprob/pdf/twocircles1.pdf
[31] T. Rappaport, *Wireless Communications: Principles and Practice*. Upper Saddle River, NJ, USA: Prentice Hall PTR, 2001.
[32] Memsic micaz sensor mote specification. [Online]. Available: http://www.memsic.com/wireless-sensor-networks/MPR2400CB
[33] Cc2420 datasheet. [Online]. Available: http://inst.eecs.berkeley.edu/cs150/Documents/CC2420.pdf
[34] T. Stoyanova, F. Kerasiotis, A. S. Prayati, and G. D. Papadopoulos, "Evaluation of impact factors on rss accuracy for localization and tracking applications in sensor networks," *Telecommunication Systems*, no. 3-4, pp. 235–248, 2009.

Noureddine Lasla is a Ph.D. student at the USTHB, Algeria. He is also a research assistant at the Research Center CERIST, Algeria. He received his M.S. degree in Computing Science from National Institute of Informatics (ESI) in 2008. His current research interest is localization, deployment and coverage in wireless sensor network.

Mohamed F. Younis is an associate professor in the Department of CSEE at the University of Maryland Baltimore County (UMBC). Before joining UMBC, he was at Honeywell International Inc. While at Honeywell, he led multiple projects for building integrated fault-tolerant avionics, in which a novel architecture and an operating system were developed. He has five granted and two pending patents. He has published more than 200 technical papers in refereed conferences and journals. He is a senior member of the IEEE.

Abdelraouf Ouadjaout is a Ph.D. student at the USTHB, Algeria. He is also a research assistant at the Research Center CERIST, Algeria. He received his M.S. degree in Computing Science from the USTHB in 2009. His current research interests are wireless sensor networks and software verification of embedded software.

Nadjib Badache Joined USTHB University of Algiers, in 1983, as assistant professor and then professor, where he taught operating systems design, distributed systems and networking with research mainly in distributed algorithms and mobile systems. From 2000 to 2008, he was head of LSI laboratory, where he conducted many projects on routing protocols, energy efficiency and security in Mobile Ad-hoc Networks and WSN. Since March, 2008 he is director of CERIST and professor at USTHB University.

APPENDIX A
PSEUDO CODE OF THE HSL ALGORITHM

Algorithm 1 Residence area of node S

let A be the set of neighbor anchors.
let HSL be the set of the half symmetric-lens areas where the node S is inside them
let CR be the set of the crescent areas where the node S is inside them
let ER be the set of the excluded regions where the node S is outside them
for each $A_i, A_j \in A$ where $A_i \neq A_j$ **do**
  if $RSSI_{A_iS} > RSSI_{A_iA_j}$ and $RSSI_{A_jS} > RSSI_{A_iA_j}$ **then**
    if $RSSI_{A_iS} > RSSI_{A_jS}$ **then**
      $HSL = HSL \cup \{HSL(A_i, A_j)\}$
    else if $RSSI_{A_jS} > RSSI_{A_iS}$ **then**
      $HSL = HSL \cup \{HSL(A_j, A_i)\}$
    end if
  else
    if $RSSI_{A_iS} > RSSI_{A_iA_j}$ **then**
      $CR = CR \cup \{CR(A_i, A_j)\}$
    else
      if $RSSI_{A_jS} > RSSI_{A_iA_j}$ **then**
        $CR = CR \cup \{CR(A_j, A_i)\}$
      else
        $ER = ER \cup \{\{C(A_i)\} \cup \{C(A_j)\}\}$
      end if
    end if
  end if
end for

APPENDIX B
GRID SCAN ALGORITHM

In order to provide an approximate residence area for very resource-constrained nodes, we present in this section the grid scan algorithm. First the initial residence area, which is defined by the vertices of the Voronoi cell, is mapped to a grid array. Basically, the smallest rectangle that contains the Voronoi cell is determined and is divided to small square-shaped cells. The set of grid cells, denoted by G, that the Voronoi cell covers are used to define the residence area. When Algorithm 1 defines the basic residence area for a node with respect to every pair of anchors (half-symmetric-lens, crescent and excluded region), the grid cells is then scanned in order to mark only those belonging to the intersection of all the defined areas for the anchor pairs. In other words, the grid-cells are eliminated from the Voronoi cell reflecting the shrinking of the residence area. In order to determine whether a cell is located inside the residence area in HSL, three distinct algorithms, namely, Algorithm 2, Algorithm 3 and Algorithm 4, are applied for half-symmetric-lens, crescent and excluded region, respectively. The final node's residence area is then defined as the set of cells kept (valid cells) after executing the grid scan algorithm. Therefore, the estimated node's position is defined as the average over all the valid cells.

Algorithm 2 Grid Scan for half symmetric-lens areas

for each $HSL(S, A_{in}, A_{out}) \in HSL$ **do**
  for each $G_k \in G$ **do**
    if $d_{A_{out}G_k} > d_{A_{in}A_{out}}$ **then**
      $G = G \backslash \{G_k\}$. $\{G_k$ is invalid$\}$
    else if $d_{A_{in}G_k} > d_{A_{out}G_k}$ **then**
      $G = G \backslash \{G_k\}$. $\{G_k$ is invalid$\}$
    end if
  end for
end for

Algorithm 3 Grid Scan for crescent areas

for each $CR(A_{in}, A_{out}) \in CR$ **do**
  for each $G_k \in G$ **do**
    if $d_{A_{out}G_k} < d_{A_{in}A_{out}}$ **then**
      $G = G \backslash \{G_k\}$. $\{G_k$ is invalid$\}$
    else if $d_{A_{in}G_k} > d_{A_{out}A_{out}}$ **then**
      $G = G \backslash \{G_k\}$. $\{G_k$ is invalid$\}$
    end if
  end for
end for

Algorithm 4 Grid Scan for excluded regions

for each $ER(A_1, A_2) \in ER$ **do**
  for each $G_k \in G$ **do**
    if $d_{A_1G_k} < d_{A_1A_2}$ **then**
      $G = G \backslash \{G_k\}$. $\{G_k$ is invalid$\}$
    else if $d_{A_2G_k} < d_{A_1A_2}$ **then**
      $G = G \backslash \{G_k\}$. $\{G_k$ is invalid$\}$
    end if
  end for
end for

B.1 Grid Scan Algorithm Performance

In this section we assess the performance of the grid scan algorithm under different grid sizes. We have conducted an extensive simulation and calculated the average size of the obtained residence areas for one node and the associate storage overhead when varying the number of anchors. The results are plotted in Figs. 16 and 17, using four different sizes of the squares that constitute the grid, namely $2, 5, 10,$ and 15 unites. We have run the simulation 100 times for each number of neighboring anchors, and the results are plotted with 95% confidence interval. The anchors are deployed inside a circle centred at node's position with radius $R = 40m$ using a uniform random distribution. The obtained results are compared with

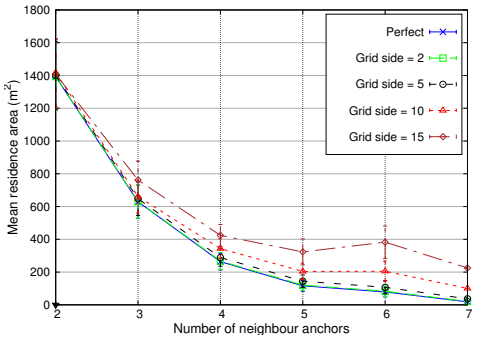

Fig. 16. Average size of the residence area for HSL using grid scan algorithm for different grid squares sizes

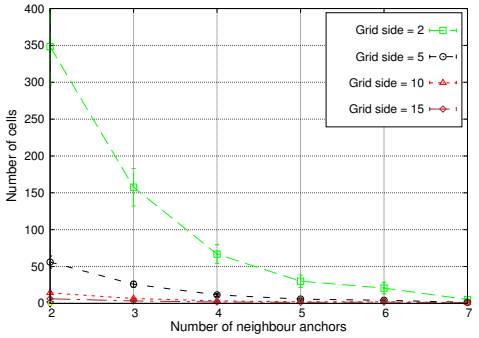

Fig. 17. Illustrating the the number of saved cells when using different grid squares sizes

the area sizes calculated using analytical geometry (available through a Python library).

Fig. 16 compares the average size of a residence area for different grid configurations and using analytical geometry (denoted perfect in the figure). The figure shows that the accuracy of the area size estimation of the grid scan improves when the cell size diminishes. While this is intuitive, the effect of the cell size is not very significant for networks with low anchor ratio.

Fig. 17 captures the storage overhead as a function of the cell size. The y-axis reports the average number of cells that is used to represent a residence area. Clearly the storage requirement will be proportional to the number of cells per residence area. The plot indicates that small cell sizes will boost the needed storage significantly. Considering both Figs 16 and 17, one can conclude that for a network with few anchors the cell size will be mostly determined by the storage constraints that a node has, i.e., using relatively large cells; while a high density of anchors will favour small cells. Based on the experiments, a cell size of 5 seems to be a reasonable choice that balances interest in both accuracy and storage resources.

APPENDIX C
ADDITIONAL SIMULATION RESULTS

Fig. 18 shows the ratio of localizable nodes in the case of log-distance path loss model. In the presence of noises, the radio signals quality and the communication range are negatively affected, which reduce the probability of receiving beacon packets from anchor nodes. In the case of obstructed factory (see Fig. 18(b)), fewer nodes are localizable compared to the case of urban area (see Fig. 18(a)). This is because in urban area less noises are introduced compared to the obstructed factory. By comparing this results to that obtained in the case of free space model (see Fig. 11), the ratio of localizable nodes is decreased and more than 20% of nodes become non-localizable.

In order to show the distribution of error, Fig. 19 plots the cumulative distribution function (CDF) of localization error for the different area-based algorithms in free space, urban area and obstructed factory setups, where the ratio of anchors if fixed to 23%. The plots are consistent with the presented results in section 5 and show the negative impact of noises on the average localization error of area based algorithms. The results also confirm the performance advantage of HSL over APIT, ROCRSSI and DRLS even in the presence of noises, as shown in Figs. 19(b) and 19(c).

In order to show the contribution of applying the Voronoi technique to the performance of HSL, Figs. 20 and 21 plot the mean error and the CDF of localization error, respectively, when such a technique is applied to all the other baseline algorithms. In other words, in both figures HSL, APIT, ROCRSSI and DRLS apply the Voronoi technique. The results clearly show that by applying the Voronoi technique to the other algorithms, the localization error decreases and better performance is obtained since more nodes become localizable and have an initial residence area (Voronoi cell). Yet HSL still sustains its performance advantage over the other algorithms even when they apply the Voronoi technique, due to the basic half symmetric lens shape used by HSL which yields smaller residence area than the other approaches.

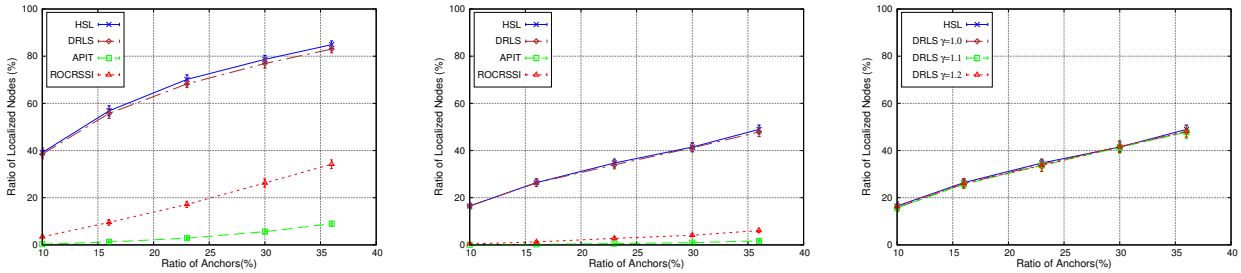

(a) (b) (c)

Fig. 18. Localizable nodes ratio assuming a log-distance path loss model in (a) urban area [$\beta = 3, \sigma = 5$], (b) obstructed factory [$\beta = 4, \sigma = 6.8$], and (c) DRLS in obstructed factory [$\beta = 4, \sigma = 6.8$]

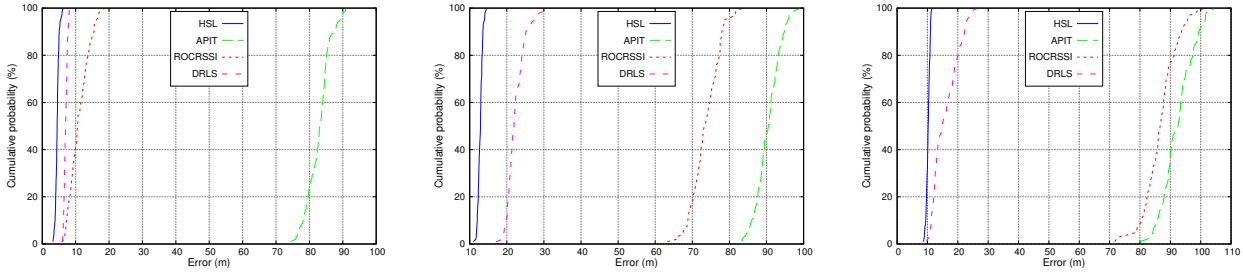

(a) (b) (c)

Fig. 19. CDF of localization error assuming (a) free space model, (b) log-distance model in urban area [$\beta = 3, \sigma = 5$] and (c) log-distance model in obstructed factory [$\beta = 4, \sigma = 6.8$]

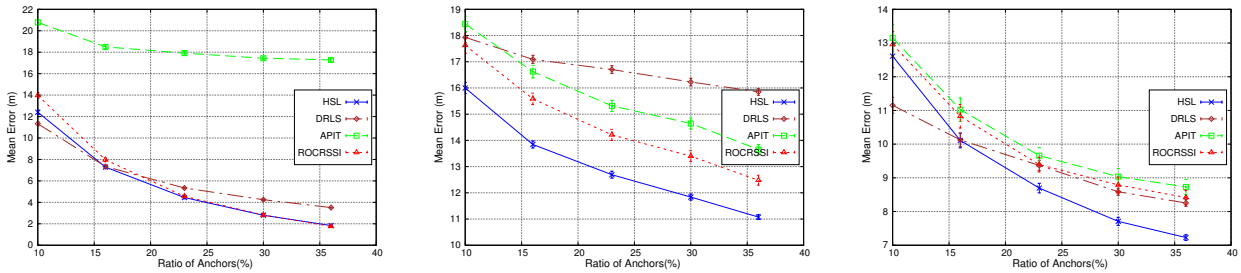

(a) (b) (c)

Fig. 20. Mean error when applying Voronoi technique to DRLS, ROCRSSI and APIT assuming (a) free space model, (b) log-distance model in urban area [$\beta = 3, \sigma = 5$] and (c) log-distance model in obstructed factory [$\beta = 4, \sigma = 6.8$]

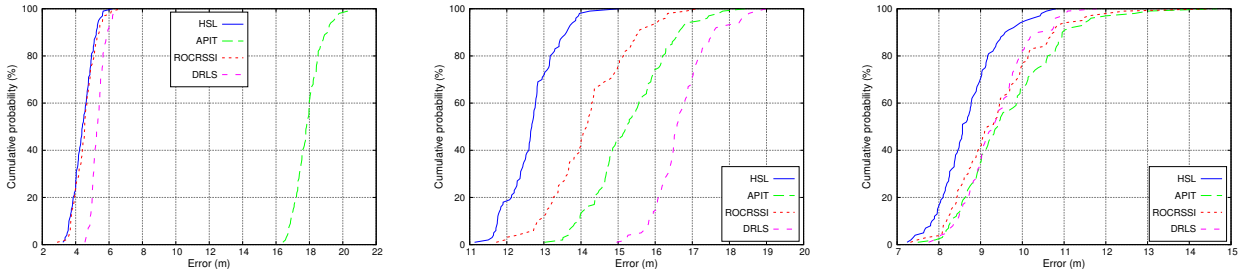

(a) (b) (c)

Fig. 21. CDF of localization error when applying Voronoi technique to DRLS, ROCRSSI and APIT in (a) free space, (b) urban area [$\beta = 3, \sigma = 5$] and (c) obstructed factory[$\beta = 4, \sigma = 6.8$]